Research Paper

Finite Element Analysis of SAW Sensor with ZnO Substrate for Dichloromethane (DCM) Gas Detection

Mohamed MOUSTAFA(1)*, Ghaylen LAOUINI(2), Tariq ALZOUBI(2)

(1) *Department of Physics, School of Sciences and Engineering, The American University in Cairo*
Egypt
*Corresponding Author e-mail: mohamed.orabi@aucegypt.edu

(2) *College of Engineering and Technology, American University of the Middle East*
Kuwait

(*received November 12, 2020; accepted April 23, 2021*)

A SAW gas sensor based on Zinc Oxide (ZnO) piezoelectric substrate is simulated and evaluated for the detection of the dichloromethane (DCM) volatile organic compound (VOC). The study is performed based on the finite element method (FEM) using COMSOL Multiphysics software. The obtained device response using the ZnO substrate is compared to the one using the typical lithium niobate ($LiNbO_3$) piezoelectric substrate. A thin film of polyisobutylene (PIB) membrane is selected to act as the sensing layer. The obtained results reveal a linear behaviour of the resonance frequency downshift (i.e., the sensor sensitivity) *versus* the investigated gas concentrations varying from 10 ppm to 100 ppm of DCM gas. Additionally, the sensor response is investigated by applying several thicknesses of PIB ranging from 0.3 μm to 1.0 μm. The observed sensor response shows less dependence on the PIB thickness using the ZnO substrate than the $LiNbO_3$ one.

Keywords: surface acoustic wave (SAW); gas sensors; VOCs; FEM modelling.

1. Introduction

The deterioration of indoor air quality (IAQ) is one of the severe problems that generally accompanies prompt urbanisation and modernisation, especially in developing countries. The poor IAQ was indicated as one of the leading causes of health and environmental problems (Deng *et al.*, 2012; Roesch *et al.*, 2014). Volatile organic compounds (VOCs) are considered one of the common indoor air pollutants. They hurt the health and evaporate quickly at room temperature. Along with carbon, they may contain other elements such as hydrogen, oxygen, fluorine, chlorine, bromine, sulfur, or nitrogen. VOCs are emitted as gases from solids or liquids, and they are characterised by high vapour pressure and low water solubility. There are thousands of different VOCs used in our daily lives affecting the air quality (Hernandez *et al.*, 2020; Sua *et al.*, 2013). Some VOCs are hazardous to human health and cause environmental damages. Among these VOCs, dichloromethane (or methylene dichloride, abbreviated herein as DCM), which is considered one of the most harmful VOCs, has received attention regarding risk reduction. DCM is a chlorinated hydrocarbon solvent that is known to be toxic to the central nervous system, subject to a high level of gas exposure (Koistinen *et al.*, 2008). Therefore, finding an approach for using sensors to detect such hazardous VOCs is of high demand and importance for the protection of a multitude of environmental and human health applications.

Gas sensors become very significant in several application areas. They are considered one of the vital devices for the supervision of indoor air quality and the detection of noxious gases. Many methods and materials have been explored to detect the VOCs, such as optical fibers (Yoon *et al.*, 2003; Jang *et al.*, 2006), localised surface plasmon resonance (LSPR) (Mombello *et al.*, 2009; Ma *et al.*, 2011), metal oxide semiconductor (MOS) sensor (Aslam *et al.*, 2018), polymer composite sensors (Hands *et al.*, 2012), carbon nanotubes (Wang *et al.*, 2009; Wongchoosuk

et al., 2010), and colorimetric sensor array (Lin *et al.*, 2011). Each of them exhibits distinguished properties as well as specific advantages and disadvantages. For example, the colorimetric sensor array devices are easy to produce, come at low cost, and make it possible to monitor different VOC gases in real time. On the other hand, their problem is that they cannot detect the concentration of VOCs. LSPR sensors showed a good sensing ability for VOC gas detection. However, they are expensive and bulky, have a complex fabrication process. Also, side-polished fiber optic sensors are bulky, have a low dynamic range associated with high response and recovery times, and showed unstable sensing performance. Surface acoustic waves (SAW) sensors have recently received considerable attention due to their remarkable advantages and characteristics. A SAW device can act as a sensor in many fields. Indeed, the SAW gas sensors were extensively studied with significant impact (Ondo *et al.*, 2020; Aslam *et al.*, 2018; Tang *et al.*, 2004; Jiang *et al.*, 2005; Leonhard *et al.*, 2004; El-Shennawy *et al.*, 2000; Liu *et al.*, 2012). They are highly sensitive and selective, compact, economically priced and cheap in maintenance, robust, reliable, reproducible, simple to handle. Additionally, they allow remote sensing and analysis in real-time with no interference by electric or magnetic fields. Besides this, they have the ability for solid state fabrication and compatibility with other modern technologies. Furthermore, using SAW sensors to detect the VOC has played a prominent role in various applications such as industrial safety, fire detection, indoor air quality, and health monitoring.

Typical SAW gas sensors are structured on a piezoelectric substrate such as quartz, $LiNbO_3$, or $LiTaO_3$. The use of SAW devices based on thin film structures, on a non-piezoelectric substrate like silicon (Si), has attracted considerable attention. The objective of the film is to excite and detect acoustic waves. Devices implemented in this way benefit from the excellent properties of the Si-based integrated with the highly developed thin film technology and their suitability for integration with other devices on the same substrate. Moreover, they benefit from the significant piezoelectric and elastic properties of the used piezoelectric layer. Among the investigated piezoelectric layers, zinc oxide (ZnO) material is considered a potential material that can be employed for SAW device applications (Huang *et al.*, 2019; Özgür *et al.*, 2005). ZnO exhibits a suitable wide bandgap of ~3.4 eV, thermal stability below 500°C, and a large exciton binding energy of about 60 meV at room temperature (Guo *et al.*, 2015). ZnO has been investigated on different materials such as ZnO/Si (Le Brizoual *et al.*, 2006), ZnO/quartz (Kumar *et al.*, 2009), and $Si/SiO_2/ZnO$ (Caliendo, Laidoudi, 2020).

In this paper, we report on detecting the DCM in the air using a SAW gas sensor based on ZnO piezoelectric substrate. The sensing behaviour of the device has been performed on COMSOL Multiphysics software. The resonance frequencies and their corresponding shifts of the device are determined using ZnO piezoelectric substrates. The results are also compared to the commonly used $LiNbO_3$ substrate. Then, for further evaluation of the device performance, the sensor response with several thicknesses of PIB ranging from 0.3 μm to 1.0 μm is presented and discussed.

2. Theoretical model and simulation methodology

The device structure was studied by a finite element method (FEM) model implemented on the COMSOL Multiphysics. FEM proved its potential as a numerical method to investigate the performance of SAW devices (El Gowini *et al.* 2010; Hofer *et al.*, 2006). The quasistatic equations for modelling piezoelectric devices are Newton's law, Gauss's law, and the constitutive relations. SAW propagation is controlled by differential equations that are solved along with the geometric complexity of the device, the material properties, and certainly while taking the boundary conditions into account. The relationship among the stress (T), strain (S), electric field (E), and electric displacement (D) of piezoelectric materials is expressed by the so called constitutive equations or equations of state of the system as below:

$$T_{ij} = C^E_{ijkl} S_{kl} - e_{kij} E_k, \tag{1}$$

$$D_i = e_{ikl} S_{kl} + \varepsilon^S_{ij} E_k, \tag{2}$$

where T_{ij} represents the stress vector, C^E_{ijkl} is the elasticity matrix [N/m^2], e_{ikl} is the piezoelectric matrix [C/m^2], ε_{ij} is the permittivity matrix [F/m], E_k is the electric field vector [V/m], S_{kl} is the strain vector, and D_i is the electrical displacement [C/m^2]. The degrees of freedom (dependent variables) are the global displacements u_1, u_2, and u_3 in the global x, y, and z directions. The electric potential is calculated by applying the Newton and Maxwell equations, where $i, j, k, l = 1, 2$, and 3:

$$\rho \frac{\partial^2 u_i}{\partial t^2} = C_{ijkl} \frac{\partial^2 u_i}{\partial x_j \partial x_l} + e_{kij} \frac{\partial^2 \varphi}{\partial x_j \partial x_l}, \tag{3}$$

$$e_{ikl} \frac{\partial^2 u_i}{\partial x_j \partial x_l} - \varepsilon_{jk} \frac{\partial^2 \varphi}{\partial x_j \partial x_l} = 0. \tag{4}$$

This study is concerned with a 2D modelling of SAW sensors based on layered structures. The potential of using 2D modelling is to reduce computational complexity. Besides that, a plane strain supposition is used for solid mechanics. Accordingly, the out of plane strain component is considered as zero. The change in

the out of plane path can be considered least if the acoustic waves are produced in the plane of the model. Most recently (Ondo *et al.*, 2020) showed the capability of applying the 2D FEM simulation for SAW sensors applications. The authors investigated the temperature influence on the performance of SAW sensors operating at gigaHertz frequency range based on Pt/AlN/sapphire structure. The results show a very good agreement between the simulation and experiments in the complete range of investigated temperatures and for all critical parameters of the SAW sensor. The geometry of the device and the periodic boundary conditions are displayed and collated in Fig. 1 and Table 1, respectively. The interdigital transducers (IDTs) are used in SAW devices to convert electrical energy to mechanical energy and vice versa. The dimensions of the SAW device used in the simulation are summarised in Table 2. The metallisation ratio is selected as 50% ($\lambda/2$). The wavelength has been chosen to be 4 μm. The material properties of Al are used from the built in COMSOL library, that is, a density of 2700 kg/m^3, Young's modulus of 70 GPa, and Poisson's ratio of 0.33. IDTs are periodic and may have hundreds of identical electrodes. Each electrode's length to width ratio can be about 100 times. Therefore, the edge effects can be neglected and reduce the model geometry to the periodic unit cell. The height of this cell should not extend to the bottom of the substrate but only a few wavelengths down. As a result, the SAW vanishes out at the lower boundary. This enforces a zero structural displacement but does not contribute to any considerable reflection from the lower boundary back into the bulk of the substrate when the surface waves are considered (Lerch, 1990). The used materials' constants employed for the simulation are collected in Table 3 (Carlotti *et al.*, 1987; Gualtieri *et al.*, 1994). The mechanical boundaries of the top and sides of both electrodes are set to be free. Additionally, the left electrode's boundaries are set to electrically ground, and the correct electrode's boundaries are set to a floating potential with zero surface charge accumulation.

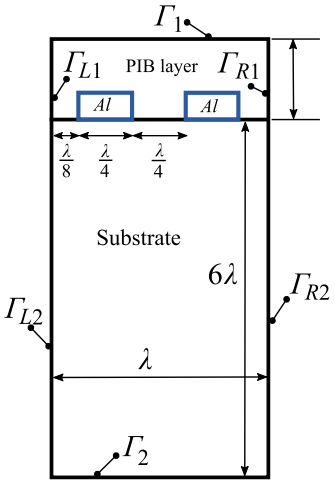

Fig. 1. Schematic representation of the studied structure, with a PIB sensing layer.

Table 1. Boundary conditions used in simulation.

Symbol	Mechanical boundary condition	Electrical boundary condition
Γ_1	Free	Zero charge/symmetry
Γ_2	Fixed	Ground
Γ_{R1}, Γ_{R2}, Γ_{L1}, Γ_{L2}	Periodic boundary condition	

Table 2. Summary of the dimensions of the device.

Structure dimensions	Value [μm]
Wavelength	4 (λ)
Pitch of electrode	2 ($\lambda/2$)
Interdigital Transducer (IDT) width	1 ($\lambda/4$)
Si substrate thickness	40 (10λ)

Table 3. Summary of $LiNbO_3$ and ZnO material constants.

	Symbol	$LiNbO_3$	ZnO
Density [kg/m^3]	ρ	4647	5720
Elastic constants [GPa]	c_{11}	203	157
	c_{12}	57.3	89
	c_{13}	75.2	83
	c_{14}	8.5	–
	c_{33}	242.4	208
	c_{44}	59.5	38
Piezoelectric constants [C/m^2]	e_{15}	3.7	0.45
	e_{22}	2.5	–
	e_{31}	0.23	0.51
	e_{33}	1.33	1.22
Dielectric constant [10^{-11} F/m]	ε_{11}	85.2	7.41
	ε_{33}	28.7	7.82

A thin film sensing layer coating is required to cover the acoustic path to determine the performance of the gas sensor. In this study, a thin film of polyisobutylene PIB is used. The PIB is favoured as a sensing film due to its low crystalline property, high permeability, low density, and good adhesion properties. Moreover, in gas sensing applications, PIB has proven to be more sensitive than other polymers (Beauchet *et al.*, 2007; Joo *et al.*, 2006). The density of the PIB film is 0.918 g/m^3, the Poisson's ratio is 0.48, and the Young's modulus is set to 10 Gpa. The adsorption of a VOC gas is represented as a slight increase of the overall density of the PIB film as:

$$\rho = \rho_{\mathrm{PIB}} + \mathrm{switch} \cdot \rho_{\mathrm{Gas,\,PIB}}. \tag{5}$$

The model is solved with a specific substrate for two cases, i.e., without and with the effect of the adsorbed

organic gas in PIB, and the value of every specific $\rho_{\text{Gas, PIB}}$ is determined. When the sensor is exposed to the organic gas in the air at atmospheric pressure and room temperature, the "partial density" of organic gas in the PIB film can be calculated as:

$$\rho_{\text{Gas, PIB}} = KMc, \tag{6}$$

where K is the air/PIB partition coefficient for every gas and M is its molar mass. The organic gas concentration (c) is estimated using the gas law:

$$c = \frac{c_o p}{RT}, \tag{7}$$

where c is in moles/m^3, c_o is the concentration in parts per million, p is the pressure, T is the temperature, and R is the gas constant. Any effects of the gas adsorption on the material properties part from the density are ignored. Periodic conditions are applied on vertical boundaries of the unit cell, implying that the wavelength of the wave must be an integer fraction of the width of the unit cell. The resonant frequency of the device is related to the spacing between the IDT and can be estimated from the following formula:

$$v_{\text{R}} = f\lambda, \tag{8}$$

where v_{R} is the Rayleigh wave velocity, f is resonant device's frequency, and λ is the wavelength of the acoustic wave.

3. Results and discussions

The SAW is an acoustic wave that propagates confined to the surface region of a piezoelectric material. It penetrates only a wavelength deep into the bulk region associated with a very high energy density at the surface. This wave is also known as the Rayleigh wave. The difference between the Rayleigh wave velocities defines a unique resonant frequency for the device to work on. This frequency is calculated from Eq. (8). The SAW phase velocity is obtained for the simulated device using ZnO substrate is 2529 m/s. This value is close to the reported experimental value for SAW in ZnO crystal film of 2675.4 m/s (Tang *et al.*, 2004). In the case of $LiNbO_3$, the velocity is reported to be 3420 m/s, which is comparable to the Rayleigh mode experimental velocity of ~3770 m/s (Tonami *et al.*, 1995). The obtained values of the velocity of SAW are reported after justifying the sufficiency of mesh density. A mesh convergence study has been conducted until the values of the velocity of SAW became constant. The mesh profiles are summarised in Fig. 2. To get accurate results for the study, the maximum number of mesh elements was chosen to be 121,657 and 4136 boundary elements. This mesh profile is not shown. This is corresponding to a working frequency of 1198764420 Hz.

Firstly, the response of the SAW device is studied with 100 ppm of DCM gas concentration. The displacement profiles of the device are illustrated in Fig. 3. Figures 3a and 3b show the obtained resonant and the anti-resonant SAW modes of the device using ZnO substrate, respectively. For a comparative study, the simulation is also performed using the same parameters for the $LiNbO_3$ substrate. The obtained results using $LiNbO_3$ substrate are shown in Figs 3c and 3d for resonant and anti-resonant SAW modes, respectively. The resonant SAW modes are presented from the point of view of total displacement. As expected, most SAWs occur at the surface, and their amplitude decreases with the depth of the material. It is also worthy to recall that the resonant SAW mode occurs due to the constructive interference of propagating waves, whereas the anti-resonant SAW mode occurs due to the destructive interference of propagating waves. The uniform wave travelling along the surface at

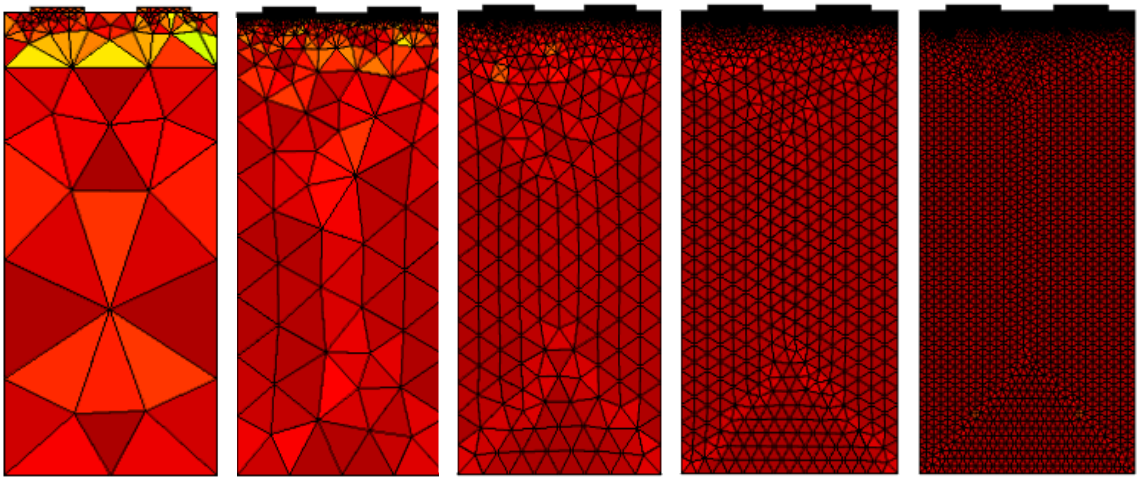

Fig. 2. Mesh density profile (from left to right) consists of domain elements of 19347, 29577, 40809, 45621, and 55374, respectively, and boundary elements of 2864, 3696, 3760, 3811, and 3894, respectively. The working frequencies are 1200121643 Hz, 1199509466 Hz, 1198909515 Hz, 1198788654 Hz, and 1198767081 Hz, respectively.

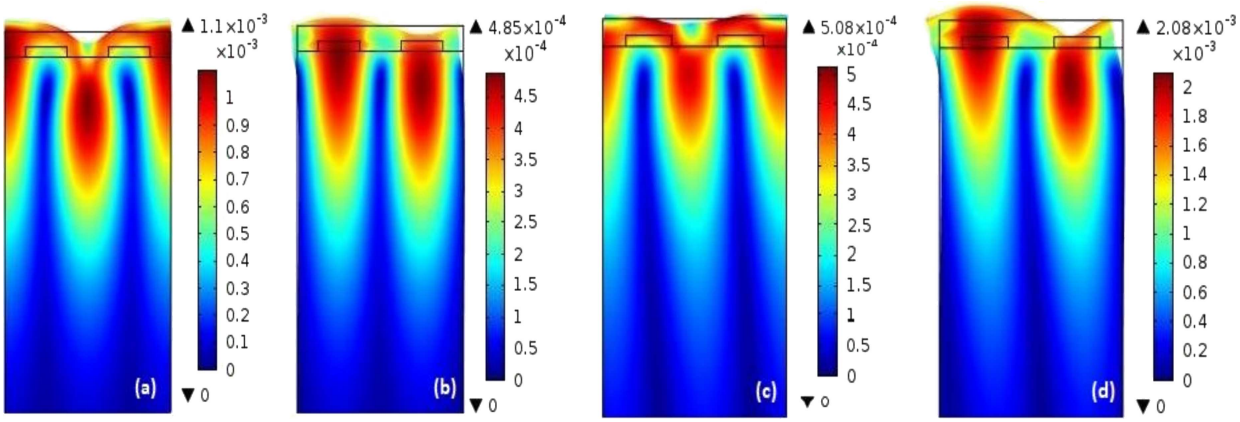

Fig. 3. Total displacement profile. Resonance (a) and antiresonance SAW modes for ZnO substrate (b). Resonance (c) and antiresonance SAW modes for ZnO substrate for $LiNbO_3$ (d).

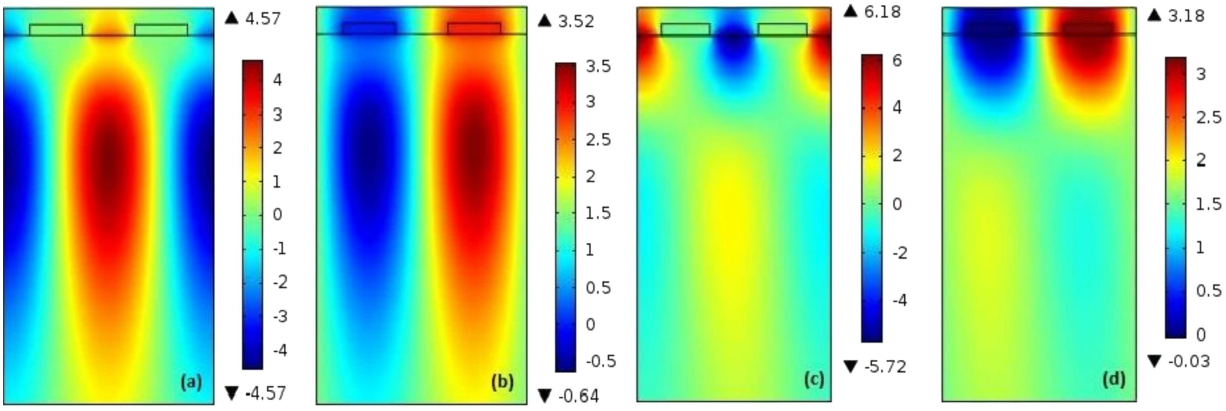

Fig. 4. Electric potential distribution using ZnO (a) and $LiNbO_3$ (c) at resonance and at the anti-resonance, again using ZnO (b) and $LiNbO_3$ (d) piezoelectric substrates.

the x-direction can be identified from the displacement strength profile. The resonance and anti-resonance frequencies using the ZnO are of values of 632 MHz and 636 MHz, respectively. These correspond to a total displacement of $1.1 \cdot 10^{-3}$ µm and $0.508 \cdot 10^{-4}$ µm. In comparison with the $LiNbO_3$, the resonance and anti-resonance frequencies are evaluated to be of 855 MHz and 849 MHz, respectively, corresponding to a total displacement of $0.485 \cdot 10^{-4}$ µm and $2.08 \cdot 10^{-3}$ µm. The total displacement in the resonance frequency of $LiNbO_3$ is observed to be a decimal lower than ZnO. On the other hand, the results show more symmetric displacement of using the ZnO substrate than that of the $LiNbO_3$ substrate. Figure 4 shows the electric potential distribution for the ZnO substrate symmetric with respect to the centre of each electrode for both substrates compared with the $LiNbO_3$ one. ZnO shows lower results between 4.57 V and −4.57 V and $LiNbO_3$ shows the highest electric potential between 6.18 V and −5.72 V.

Detection of gas concentrations in the parts per million level [ppm] is pivotal for crucial applications such as environmental monitoring. Hence, the sensitivity of the SAW structures with the $LiNbO_3$ and ZnO in resonance frequency shift under exposure to DCM gas with concentration is simulated and discussed. The device has been exposed to air containing DCM concentration ranging from 10 ppm to 100 ppm. The adsorbed DCM increases the PIB mass density and lowers the phase velocity and consequently the operating frequency, which can be correlated to the investigated gas concentration. Figure 5 illustrates the dependence of the resonance frequency shift on the DCM

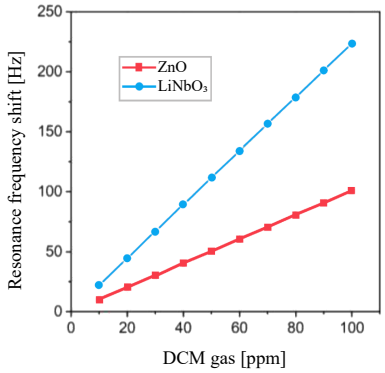

Fig. 5. Resonance frequency shift *versus* the DCM gas concentration, for both ZnO and $LiNbO_3$ piezoelectric substrates.

gas concentration. The frequency shift Δf of the device can be calculated as $\Delta f = f - f_o$, where f and f_o are the resonance frequencies after and the corresponding value before the explosion to the gas, respectively (i.e., a negative value). However, for a more convenient reading of the graph, the magnitude of the frequency shift is plotted *versus* the gas concentration (see Fig. 5). A comparison with the results obtained using the $LiNbO_3$ substrate is given on the same plot. The points represent the simulated frequency shift values due to the exposure of the gas, while the straight line represents the fit of the results. For both substrates, the shift in frequency increases in magnitude with the increase of the DCM concentration. The highest frequency shifts are reported with 100 Hz and 224 Hz values, with a gas concentration of 100 ppm, for the ZnO and $LiNbO_3$, respectively. Further, from the sensing response of the sensor device, it can be observed that the frequency shift reveals a linear proportionality to the DCM concentration over the range of the gas concentration under investigation. This linearity characteristic is a vital finding for the employment of SAW devices in sensing applications. The observed sensing performance is consistent with earlier experimentally observed performance of other SAW sensors using different sensing systems for several VOC gases like dimethylamine, ethanol, and acetic acid VOCs based on other structures, e.g., the ZnO/SiO_2/Si-based SAW sensor (Horrillo *et al.*, 2006).

Moreover, the slope of the response of the device using the $LiNbO_3$ substrate, i.e., the sensitivity of the proposed sensing system, was higher than that using the ZnO one. Values of 2.23595 Hz/ppm slope for $LiNbO_3$ structure and 1.00835 Hz/ppm slope for ZnO structure are reported. The linear dependence of the gas concentration proposes a sensing system with a wide dynamic range. This characteristic is of vital importance for the employment of such devices in gas sensing applications. Figure 6 shows the effect of the thickness of the PIB sensing layer (from 0.3 μm to 1.0 μm) on the frequency shift at 100 ppm of DCM. Increasing the thickness of PIB leads to an increase in the shift in frequency. For $LiNbO_3$, we observe an increase in linear growth from 69.667 Hz to 119.448 Hz, unlike ZnO, which shows a minor increase from 139.014 Hz to 433.011 Hz, varying the PIB thickness from 0.3 μm to 1.0 μm, respectively. Therefore, it can be concluded that the device behaviour using the ZnO substrate, rather than using the $LiNbO_3$, is less dependent on the PIB thickness. Indeed, it is desirable to generate high-quality and single-crystalline ZnO nanostructures for chemical sensing applications based on ZnO nanomaterials. Besides this, the ZnO thin film substrates are more compatible with the integrated circuit technology and semiconducting manufacturing. As the study is concerned with the use of $LiNbO_3$ in comparison with ZnO piezoelectric substrates for SAW gas sensing application, the results can be further interpreted as described. However, the former processes a more significant resonance frequency and higher sensitivity to DCM, its temperature coefficient of frequency (TCF) is quite large (Horrillo *et al.*, 2006). The ZnO is a versatile material exhibiting low TCF, a wide bandgap characteristic (~3.37 eV at room temperature), excellent bonding on various substrates, and high electrical resistivity (Tonami *et al.*, 1995; Raj *et al.*, 2017; Ondo-Ndong *et al.*, 2002). These parameters should be taken into consideration while producing a SAW sensor for applications.

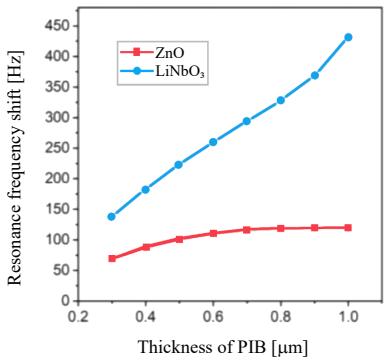

Fig. 6. Resonance frequency shift *versus* the thickness of the PIB sensing layer using both ZnO and $LiNbO_3$ piezoelectric substrates.

4. Conclusions

A SAW gas sensor for the DCM-VOC gas detection has been investigated by the COMSOL Multiphysics package using the ZnO as a piezoelectric substrate. The sensor's response using the ZnO substrate is compared to that of the $LiNbO_3$. The results indicate a linear dependence of the frequency shift on the gas concentration when the device is exposed to a concentration from 10 ppm to 100 ppm. This characteristics is vital for the employment of such devices in sensing applications. Additionally, the sensor response is analysed at different thicknesses of the PIB sensing layer. The results reveal that the response of the sensor using ZnO is less affected by the change in the PIB thickness than that using $LiNbO_3$. For example, at PIB thickness of 400 nm, the frequency shifts are evaluated about 90 Hz and 170 Hz for the ZnO and $LiNbO_3$ substrates, respectively. The study demonstrates the potential of SAW gas sensors for health and environmental applications.

References

1. Aslam M.Z., Jeoti V., Karuppanan S., Malik A., Iqbal A. (2018), FEM analysis of Sezawa Mode SAW sensor for VOC based on CMOS compatible AlN/SiO_2/Si, *Multilayer Structure. Sensors*, **18**(6): 1687, doi: 10.3390/s18061687.

2. Beauchet R., Magnoux P., Mijoin J. (2007), Catalytic oxidation of volatile organic compounds (VOCs) mixture (isopropanol/O-xylene) on zeolite catalysts, *Catalysis Today*, **124**(3–4): 118–123, doi: 10.1016/j.cattod.2007.03.030.

3. Caliendo C., Laidoudi F. (2020), Experimental and theoretical study of multifrequency surface acoustic wave devices in a single $Si/SiO_2/ZnO$ piezoelectric structure, *Sensors*, **20**(5): 1380, doi: 10.3390/s20051380.

4. Carlotti G., Socino G., Petri A., Verona E. (1987), Elastic constants of sputtered ZnO films, *Proceedings of IEEE 1987 Ultrasonics Symposium*, pp. 295–300, doi: 10.1109/ULTSYM.1987.198972.

5. Deng Q., Yang X., Zhang J.S. (2012), Key factor analysis of VOC sorption and its impact on indoor concentrations: the role of ventilation, *Building and Environment*, **47**: 182–187, doi: 10.1016/j.buildenv.2011.07.026.

6. El-Shennawy K., Orabi M.S, Taha T.E. (2000), Simulation of high sensitivity and stability surface acoustic wave NO_2 gas sensor based on amplitude variations as measurand, *22nd International Conference on Microelectronics*, Vol. 2, pp. 611–614.

7. Gowini M., Moussa W. (2010), A Finite Element Model of a MEMS-based Surface Acoustic Wave hydrogen sensor, *Sensors*, **10**(2): 1232–1250, doi: 10.3390/s100201232.

8. Gualtieri J.G., Kosinski J.A., Ballato A. (1994), Piezoelectric materials for acoustic wave applications, *IEEE Transactions on Ultrasonics, Ferroelectrics, and Frequency Control*, **41**(1): 53–59, doi: 10.1109/58.265820.

9. Guo Y.J. *et al.* (2015), Ultraviolet sensing based on nanostructured ZnO/Si surface acoustic wave devices, *Smart Materials and Structures*, **24**(12): 125015, doi: 10.1088/0964-1726/24/12/125015.

10. Hands P.J.W., Laughlin P.J., Bloor D. (2012), Metal–polymer composite sensors for volatile organic compounds. Part 1. Flow-through chemi-resistors, *Sensors and Actuators B: Chemical*, **162**(1): 400–408, doi: 10.1016/j.snb.2011.12.016.

11. Hernandez G., Wallis S.L., Graves I., Narain S., Birchmore R., Berry T-A. (2020), The effect of ventilation on volatile organic compounds produced by new furnishings in residential buildings, *Atmospheric Environment: X*, **6**: 10069, doi: 10.1016/j.aeaoa.2020.100069.

12. Hofer M. *et al.* (2006), Finite-element simulation of wave propagation in periodic piezoelectric SAW structures, *IEEE Transactions on Ultrasonics, Ferroelectrics, and Frequency Control*, **53**(6): 1192–1201, doi: 10.1109/tuffc.2006.1642518

13. Horrillo M.C. *et al.* (2006), Optimization of SAW sensors with a structure ZnO-SiO2-Si to detect volatile organic compounds, *Sensors and Actuators B: Chemical*, **118**(1–2): 356–361, doi: 10.1016/j.snb.2006.04.050.

14. Huang H., Chiang H., Wu C., Lin Y., Shen Y. (2019), Analysis on characteristics of ZnO surface acoustic wave with and without micro-structures, *Micromachines (Basel)*, **10**(7): 434, doi: 10.3390/mi10070434.

15. Jang S.W. *et al.* (2006), Refractive index change by photoinduction of a UV-sensitive SMF-to-PWG coupler. *IEEE Photonics Technology Letters*, **18**(1): 220–222, doi: 10.1109/LPT.2005.861624.

16. Jiang Q., Yang X.M, Zhou H.G, Yang J.S. (2005), Analysis of surface acoustic wave pressure sensors, *Sensors and Actuators A: Physical*, **118**(1): 1–5, doi: 10.1016/j.sna.2004.07.007.

17. Joo B.-S., Lee J.-H., Lee E.-W., Song K.-D., Lee D.-D. (2005), Polymer film SAW sensors for chemical agent detection, [in:] *Proceedings of the 1st Conference on Sensing Technology*, Palmerston North, New Zealand, pp. 307–310.

18. Karpina V.A. *et al.* (2004), Zinc oxide – analogue of GaN with new perspective possibilities, *Crystal Research and Technology*, **39**(11): 980–992, doi: 10.1002/crat.200310283.

19. Koistinen K. *et al.* (2008), The INDEX project: executive summary of a European Union project on indoor air pollutants, *Allergy*, **63**(7): 810–819, doi: 10.1111/j.1398-9995.2008.01740.x.

20. Kumar S., Kim G.H., Sreenivas K., Tandon R.P. (2009), ZnO based surface acoustic wave ultraviolet photo sensor, *Journal of Electroceramics*, **22**(1): 198–202, doi: 10.1007/s10832-007-9409-7.

21. Lin H., Jang M., Suslick K.S. (2011), Preoxidation for colorimetric sensor array detection of VOCs, *Journal of the American Chemical Society*, **133**(42): 16786–16789, doi: 10.1021/ja207718t.

22. Le Brizoual L., Elmazria O., Sarry F., El Hakiki M., Talbi A., Alno P. (2006), High frequency SAW devices based on third harmonic generation, *Ultrasonics*, **45**(1–4): 100–103, doi: 10.1016/j.ultras.2006.07.013.

23. Leonhard M., Ismail M. (2004), Wireless measurement of temperature using surface acoustic waves sensors, *IEEE Transactions on Ultrasonics, Ferroelectrics, and Frequency Control*, **51**(11): 1457–1463, doi: 10.1109/TUFFC.2004.1367486.

24. Lerch R. (1990), Simulation of piezoelectric devices by two- and three-dimensional finite elements, *IEEE transactions on Ultrasonics, Ferroelectrics, and Frequency Control*, **37**(3): 233–247, doi: 10.1109/58.55314.

25. Liu X., Cheng S., Liu H., Hu S., Zhang D., Ning H. (2012), A survey on gas sensing technology, *Sensors (Basel)*, **12**(7): 9635–9665, doi: 10.3390/s120709635.

26. Ma W., Yang H., Wang W., Gao P., Yao J. (2011), Ethanol vapor sensing properties of triangular silver nanostructures based on localized surface plasmon resonance, *Sensors*, **11**(9): 8643–8653, doi: 10.3390/s110908643.

27. Mombello D. *et al.* (2009), Porous anodic alumina for the adsorption of volatile organic compounds, *Sensrs and Actuators B: Chemical*, **137**(1): 76–82, doi: 10.1016/j.snb.2008.11.046.

28. Ondo-Ndong R., Ferblantier G., Al Kalfioui M., Boyer A., Foucaran A. (2002), Properties of RF magnetron sputtered zinc oxide thin films, *Journal of Crystal Growth*, **255**(1–2): 130–135, doi: 10.1016/S0022-0248(03)01243-0.

29. Ondo J., Blampain E., Mbourou G., Mc Murtry S., Hage-Ali S., Elmazria O. (2020), FEM modeling of the temperature influence on the performance of SAW sensors operating at gigahertz frequency range and at high temperature up to 500°C, *Sensors (Basel)*, **20**(15): 4166, doi: 10.3390/ s20154166.

30. Özgür Ü. *et al.* (2005), A comprehensive review of ZnO materials and devices, *Journal of Applied Physics*, **98**(4): 041301, doi: 10.1063/1.1992666.

31. Raj V.B., Singh H., Nimal A.T., Sharma M.U., Tomar M., Gupta V. (2017), Distinct detection of liquor ammonia by ZnO/SAW sensor: Study of complete sensing mechanism, *Sensors and Actuators B: Chemical*, **238**: 83–90, doi: 10.1016/j.snb.2016.07.040.

32. Roesch C., Kohajda T., Roeder S., von Bergen M., Schlink U. (2014), Relationship between sources and patterns of VOCs in indoor air, *Atmospheric Pollution Research*, **5**(1): 129–137, doi: 10.5094/APR.2014.016.

33. Sua F.-C., Mukherjeeb B., Battermana S. (2013), Determinants of personal, indoor and outdoor VOC concentrations: An analysis of the RIOPA data, *Environmental Research*, **126**: 192–203, doi: 10.1016/j.envres.2013.08.005.

34. Tang I.-T., Chen H.-J., Hwang W.C., Wang Y.C., Houng M.-P., Wang Y.-H. (2004), Applications of piezoelectric ZnO film deposited on diamond-like carbon coated onto Si substrate under fabricated diamond SAW filter, *Journal of Crystal Growth*, **262**(1–4): 461–466, doi: 10.1016/j.jcrysgro.2003.10.081.

35. Tonami S., Nishikata A., Shimizu Y. (1995), Characteristic of leaky surface acoustic wave propagating on $LiNbO_3$ and $LiTaO_3$ substrates, *Japanese Journal of Applied Physics*, **34**(Part 1, No. 5B): 2664–2667, doi: 10.1143/jjap.34.2664.

36. Wang Z.L. (2004), Zinc oxide nanostructures: growth, properties and applications, *Journal of Physics: Condensed Matter*, **16**(25): R829–R858, doi: 10.1088/0953-8984/16/25/R01.

37. Wongchoosuk C., Wisitsoraat A., Tuantranont A., Kerdcharoen T. (2010), Portable electronic nose based on carbon nanotube-SnO_2 gas sensors and its application for detection of methanol contamination in whiskeys, *Sensors and Actuators B: Chemical*, **147**(2): 392–399, doi: 10.1016/j.snb.2010.03.072.

38. Yoon J.K., Seo G.W., Cho K.M., Kim E.S., Kim S.H., Kang S.W. (2003), Controllable in-line UV sensor using a side-polished fiber coupler with photofunctional polymer, *IEEE Photonics Technology Letters*, **15**(6): 837–839, doi: 10.1109/LPT.2003.811341.